Supplement of

East Asian methane emissions inferred from high-resolution inversions of GOSAT and TROPOMI observations: a comparative and evaluative analysis

Ruosi Liang et al.

Correspondence to: Yuzhong Zhang (zhangyuzhong@westlake.edu.cn)

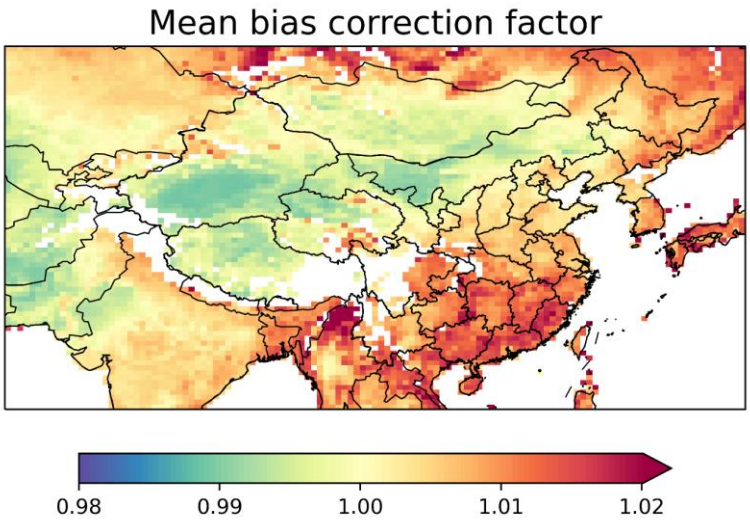

Figure S1: Bias correction factor derived by Lorente et al. (2021) for original TROPOMI XCH_4 retrievals.

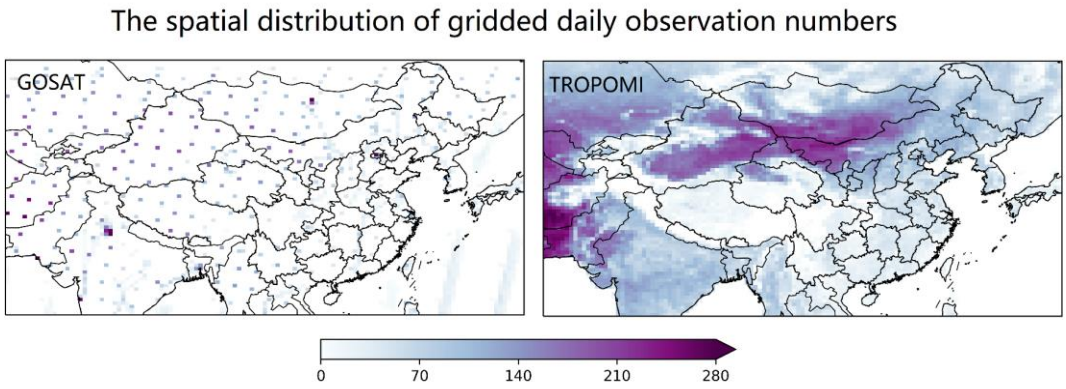

Figure S2: Numbers of gridded daily average observations for GOSAT and TROPOMI during 2019.

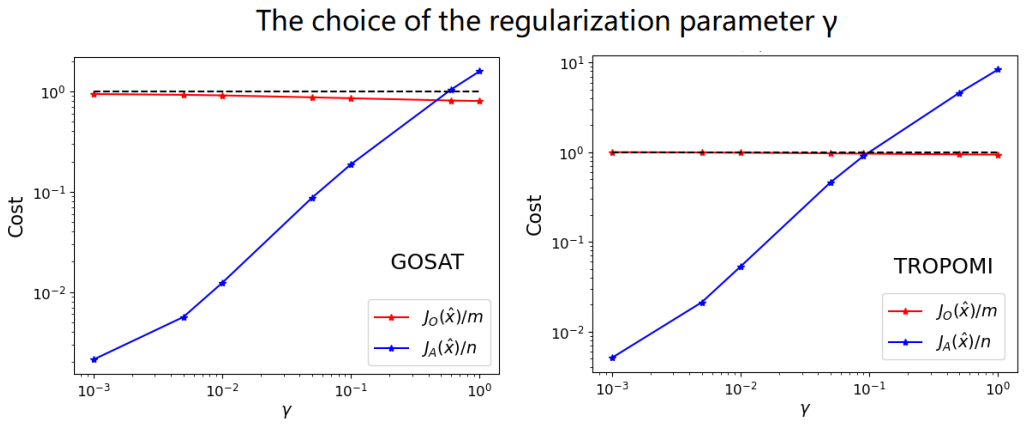

Figure S3: Determination of the regularization parameter by finding the crossing point of $J_A(\hat{x}) = (\hat{x} - x_A)^T S_A^{-1}(\hat{x} - x_A)$ and $J_O(\hat{x}) = (y - K\hat{x})^T S_O^{-1}(y - K\hat{x})$. n is the dimension of the state vector and m is the dimension of the observation vector. Left panel is for the GOSAT inversion and right panel for the TROPOMI inversion.

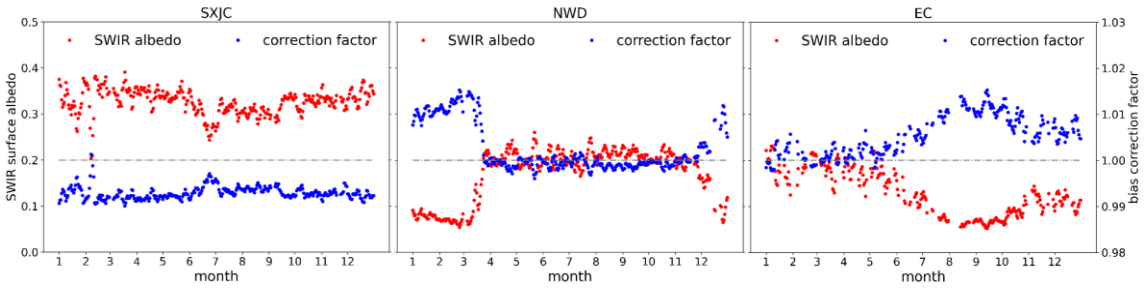

Figure S4: Time series of average surface albedo and bias correction factor over SXJC, NWD and EC. The bias correction algorithm used in this TROPOMI product is a function of the SWIR effective surface albedo where the correction is forced to be zero at surface albedo around 0.2. When the surface albedo is less than 0.2, there is a bias correction factor greater than 1, and conversely, the bias correction factor is less than 1.

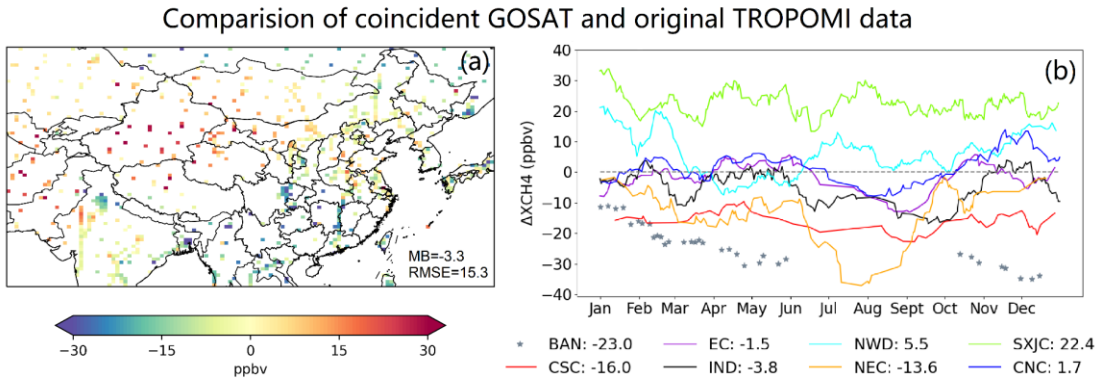

Figure S5: Average differences in XCH_4 between GOSAT and original (not bias-corrected) TROPOMI (TROPOMI-GOSAT) shown on the 0.5° × 0.625° grid (a) and by region (b). Annual averages of regional differences (in ppbv) are inset in Panel (b).

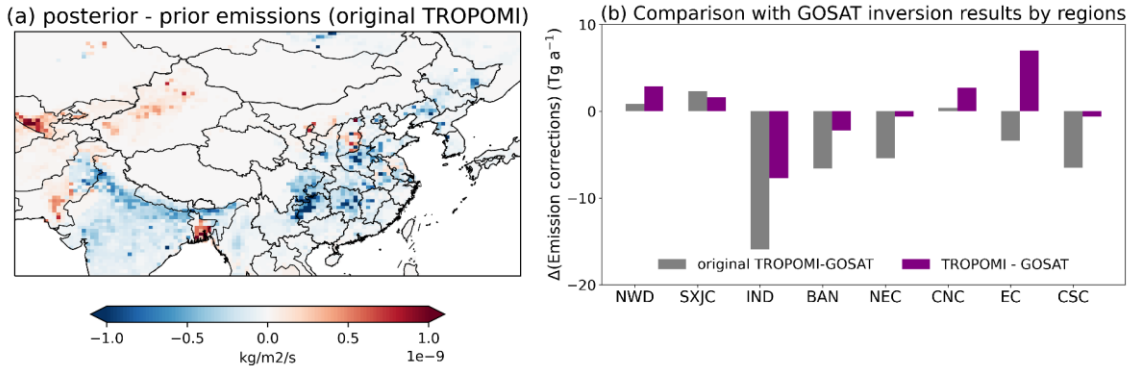

Figure S6: Results of inversions of original TROPOMI retrievals without application of the bias correction scheme. Panel (a) shows the adjustment to prior emissions by this inversion. Panel (b) compares regional inversion results using original and bias-corrected TROPOMI data, relative to the GOSAT inversion results.

Table S1: Surface observation sites used for evaluation

Site	Code	Lon	Lat	Alt(m)	Measurements
Anmyeon-do, South Korea	AMY	126.33	36.54	87	Hourly & daily, *in situ*
Pha Din, Vietnam	PDI	103.52	21.57	1478	Hourly & daily, *in situ*
Lulin, Taiwan China	LLN	120.87	23.47	2867	Weekly, flask
Ulaan Uul, Mongolia	UUM	110.10	44.45	1012	Weekly, flask
Waliguan, China	WLG	100.89	36.29	3815	Weekly, flask
Xianghe, China	XH	116.96	39.75	36	Hourly & daily, FTIR total column measurements
Hefei, China	HF	117.17	31.9	-	Hourly & daily, FTIR total column measurements

Table S2: Mean 2019 methane emissions used in GEOS-Chem[a]

Sources Type (Tg a^{-1})	**China[b]**			**East Asia[c]**		
	Prior	Posterior		Prior	Posterior	
		TROPOMI	GOSAT		TROPOMI	GOSAT
Anthropogenic						
Oil	1.0	1.6	1.2	1.5	2.1	1.8
Gas	0.2	0.2	0.2	3.6	3.7	3.9
Coal	16.6	18.0	16.2	19.4	22.1	18.7
Livestock	11.9	13.1	12.7	36.6	36.9	41.6
Landfill	2.9	3.2	2.7	5.1	5.6	5.7
Wastewater	8.1	9.0	8.1	16.0	17.1	18.0
Rice	14.5	17.1	15.9	24.8	29.6	30.0
Others	6.1	6.9	6.1	9.6	10.3	10.3
Natural						
Biomass burning	0.3	0.3	0.3	1.8	2.1	2.3
Wetlands	3.2	4.1	3.6	9.1	11.2	11.1
Seeps	0.3	0.5	0.3	0.7	0.9	0.7
Termites	0.8	0.9	0.9	1.8	1.9	2.1
Total source[d]						
Anthropogenic	61.3	69.1±0.9	63.0±0.9	116.7	127.4±1.2	130.0±1.1
Natural	4.5	5.8±0.2	5.1±0.2	13.4	16.1±0.3	16.2±0.3
All	65.8	74.9±1.0	68.1±1.0	130.0	143.5±1.4	146.2±1.2

[a] Mean 2019 values of methane sources in China and the whole inversion domain. It contains prior emissions described above and posterior emissions obtained by two inversions using TROPOMI and GOSAT observations respectively.

[b] Methane emissions in China.

[c] Methane emissions in the entire East Asian domain.

[d] Uncertainties are showed here (1σ standard deviations derived from posterior error covariance matrices).